

Discrete Molecular Dynamics Study of wild-type and Arctic-mutant (E22G) $A\beta_{16-22}$ Folding and Aggregation

Sijung Yun^{1*}, Shouyong Peng^{1†}, Luis Cruz¹, Sergey V. Buldyrev²
David B. Teplow³, H. Eugene Stanley¹ and Brigitte Urbanc¹

February 29, 2008

¹ Center for Polymer Studies and Department of Physics, Boston University,
Boston, MA 02215

² Department of Physics, Yeshiva University, New York, NY 10033

³ Department of Neurology, David Geffen School of Medicine, and Brain Research Institute and Molecular Biology Institute, University of California, Los Angeles, CA 90095

*Corresponding author. Email: yuns@mail.nih.gov

†Present addresses: Laboratory of Cell Biology, National Cancer Institute, National Institutes of Health, Bethesda, MD 20892

‡Harvard-Partners Center for Genetics and Genomics, Brigham & Women's Hospital, Boston, MA, 02115

ABSTRACT

Substantial clinical and experimental evidence supports the hypothesis that amyloid β -protein ($A\beta$) forms assemblies with potent neurotoxic properties that cause Alzheimer's disease (AD). Therapeutic targeting of these assemblies would be facilitated by the elucidation of the structural dynamics of $A\beta$ aggregation at atomic resolution. We apply the *ab initio* discrete molecular dynamics approach coupled with a four-bead peptide model to study the aggregation of wild-type and Arctic-mutant (E22G) $A\beta_{16-22}$, a peptide that contains the $A\beta$ central hydrophobic cluster, Leu₁₇-Ala₂₁, that plays an important role in $A\beta$ assembly. The aggregation of sixteen wild-type $A\beta_{16-22}$ peptides is studied systematically under solvent conditions incorporating: (i) effective hydrophobic and electrostatic interactions; (ii) no effective hydrophobic interactions; and (iii) no effective electrostatic interactions. We find that at physiological temperatures initially-separated peptides aggregate into fibrillar units under condition (i). These units comprise multi-layered β -sheets with cross- β structure and an antiparallel arrangement of β -strands. Under condition (iii), β -strands are arranged either in a parallel or antiparallel manner, suggesting that electrostatic interactions control β -sheet organization. For condition (ii), no fully-formed fibrillar aggregates are observed, only occasional antiparallel β -strands. Fibrillar aggregates of Arctic-mutant $A\beta_{16-22}$ peptides have parallel as well as antiparallel β -strands resembling the aggregates of wild-type $A\beta_{16-22}$ peptides with no electrostatic interaction. We find that flexibility of peptide backbone is an important factor required for fibrillization. Arctic-mutant $A\beta_{16-22}$ peptides oligomerize slower due to negligible role of electrostatic interaction in driving oligomerization, but fibrillize faster due to greater flexibility and ease of rearrangement with smaller volume and no charge of G22 than wild-type. It implies that electrostatic interaction cooperatively drives initial oligomerization of $A\beta$ with hydrophobic interaction.

Keywords: Alzheimer's disease, amyloid β -protein, discrete molecular dynamics simulations, cross- β structure

Introduction

Neurodegenerative diseases such as Alzheimer's disease (AD), Parkinson's disease, and prion diseases share certain features, including protein misfolding and aggregation (1). AD is the most prevalent among these diseases and is also the most common cause of late life dementia (2). According to the revised amyloid cascade hypothesis (3), AD results from the aberrant assembly of the amyloid β -protein ($A\beta$), leading to direct peptide-mediated neurotoxic effects as well as a cascade of associated injurious physiologic events. The first assembly process recognized in AD was amyloid plaque formation (4, 5). Plaques comprise dense deposits of insoluble $A\beta$, organized into stable fibrils, and numerous other proteinaceous and nonproteinaceous macromolecules. Therapeutic efforts over the last century have focused on fibril elimination and prevention. Recent studies of fibril formation have revealed an increasing number of prefibrillar, oligomeric assemblies that are potent neurotoxins and may be the proximate effectors of AD neuropathology (3, 6–10). In fact, senile plaque formation may be an end-stage event in AD, or may even be protective (11–13). Arctic mutation (E22G) of $A\beta$, a familiar AD, cause early-onset of AD. *In vitro* studies have shown that Arctic-mutant $A\beta$ exhibits faster protofibril and fibril formation than wild-type $A\beta$ (13–18). It is important to understand structural features of fibrils and assembly mechanisms of wild-type $A\beta$ and the reason why Arctic-mutant $A\beta$ shows accelerated protofibril and fibril formation at atomic resolution to understand the toxicity of pre-fibrillar assemblies, and to prevent the formation of toxic intermediates.

Traditional all-atom molecular dynamics (MD) simulations using realistic force fields in physiological solutions require immense computational power and are thus currently limited to time scales ($\sim 10^{-6}$ s) insufficient to study *ab initio* $A\beta$ aggregation ($\gg 1$ s) (19). However, coarse-grained protein models with simplified interactions can accelerate simulations of protein folding and aggregation without losing the ability to reveal key mechanistic features of the process (20, 21). Coarse-grained protein models with discrete molecular dynamics (DMD) algorithms have been applied to the study of protein folding and aggregation (22–28). A two-bead protein model has been applied to the study of the Src SH3 domain (26, 29), c-Crk SH3 domain (30), and $A\beta$ 1-40 peptide (31). A four-bead protein model has been applied to the study of polyalanine (32) and $A\beta$ 1-40 and $A\beta$ 1-42 peptides (27, 28, 33). A coarse-grained protein model with more side-chain details has been applied to the

study of Trp-cage (34). A united-atom model, where all the atoms except hydrogens are modeled explicitly, has been applied to study folding events of $A\beta$ 21–30 (35).

$A\beta$ 16–22 is a useful peptide for studying $A\beta$ folding and assembly because it is one of the shortest $A\beta$ fragments that forms fibrils *in vitro* and it contains the central hydrophobic cluster, Leu₁₇–Ala₂₁, that plays an important role in fibril formation by full-length $A\beta$ (36, 37). $A\beta$ 16–22 has been studied *in vitro* (38–43) and *in silico* (21, 44–56). Solid-state NMR reveals that $A\beta$ 16–22 forms well-ordered, antiparallel fibrils under physiological conditions (38, 41). A dock-lock mechanism for $A\beta$ 16–22 fibrillization was suggested, based on experimental evidence (39), and was shown by using computational studies (54, 55). Hydrophobic driven coalescence followed by reorganization due to interchain hydrogen bonding interactions is proposed as another mechanism of $A\beta$ 16–22 fibrillization (56). Experimental evidence for the reorganization of β -strands within $A\beta$ 16–22 aggregates was reported (43), and a dry steric zipper (57) was proposed as a major force to stabilize the association of antiparallel layers of β -sheets for amyloid fibrils (58).

All-atom molecular dynamics simulations of $A\beta$, which have been used to test the stability of structural models based on experimental results (44), would be an ideal tool for revealing how monomers aggregate into extended β -sheets comprising fibrils. However, due to their high computational cost, they are limited to tests of stability (52) or small systems of $A\beta$ 16–22 (45–47), or they require use of a fibrillar template (54, 55) (for a review of computational approaches to $A\beta$ folding and aggregation, see (59)).

Recently, an *ab initio* discrete molecular dynamics (DMD) approach was introduced for studying $A\beta$ folding and aggregation (60). A DMD approach combined with a four-bead protein model with backbone hydrogen bonding (32) and amino acid-specific interactions due to hydropathy was shown to capture the essential differences between $A\beta$ 1–40 and $A\beta$ 1–42 oligomer formation (27, 28). Here we apply the same approach with a four-bead model to study folding of wild-type $A\beta$ 16–22 peptide and aggregation of sixteen wild-type and Arctic-mutant (E22G) $A\beta$ 16–22 peptides. In the four-bead model, each amino acid is represented by up to four “beads,” with three beads representing the protein backbone and the fourth bead representing the amino acid side-chain. We introduce a new scheme of implementing the amino acid-specific interactions among the side-chain beads by taking into account all the side-chain atoms (except hydrogens) and their hydropathic properties. Consequently, an amino acid such as Lys will interact electrostatically with

other charged side chains and also will be involved in attractive hydrophobic interaction with other hydrophobic side-chains, such as Leu and Val.

Methods

Discrete molecular dynamics (DMD)

When all interactions between particles in a system are simplified to square-well potentials or their combinations, a DMD algorithm can be applied to simulate the dynamics of the system. In DMD, each particle in the system only experiences “collisions” (elastic and/or inelastic) at distances where their interaction potential changes. Between consecutive collisions at times t_i and t_j , all particles move along straight lines with constant velocities. The DMD algorithm keeps track of the state for each particle and maintains a set of all possible collisions, a collision table, and then determines the pair of particles colliding first. If the particles p and q collide at time t_j , the states of the two particles will change according to the laws of energy and momentum conservation, and the time will be set to t_j . Then all the outdated collision events related to p and q will be updated for calculating the new possible collisions involving p or q . These new possible collisions will be inserted into the collision table to find the next collision event. Therefore, at each collision event, only the velocities of the involved pair of particles need to be updated to keep track of their new states while the rest of the system remains intact. (For reviews on details and limitations of DMD algorithm, see Refs. (60).)

The speed of the most efficient DMD algorithm is inversely proportional to $N \ln N$, where N is the total number of atoms (61), and the speed decreases linearly with the number of square-well discontinuities in the potential and the particle density. Combined with a coarse-grained protein model, the DMD algorithm is computationally more efficient compared to the traditional all-atom MD method because: (1) positions and velocities are updated only for particles experiencing collisions; (2) solvent is not explicitly present, which significantly reduces the number of particles in the system; and (3) the number of atoms in the peptide is reduced further through coarse-graining.

We perform DMD simulations in the canonical ensemble (NVT). The temperature T of a system is defined by the kinetic energy of the system,

$$\frac{3}{2}k_B T \equiv \frac{1}{N} \sum_{i=1}^N \frac{mv_i^2}{2}, \quad (1)$$

where N is number of particles in the system, m is particle mass, v_i is particle velocity, and k_B is Boltzmann's constant.

We use the Berendsen thermostat algorithm (62) to maintain the temperature of the system, through coupling the system to an external bath. We assume that the initial temperature of the system is T_i , the final temperature (i.e., the temperature of the heat bath) is T_f , and the heat exchange rate is α ($\alpha = 10^{-4}$ in our simulations unless specified). We “update” the temperature at a regular small time interval δt ,

$$T(t + \delta t) - T(t) = [T_f - T(t)]\alpha\delta t. \quad (2)$$

The system will approach the final temperature exponentially:

$$T(t) = T_f + (T_i - T_f)e^{-\alpha t}. \quad (3)$$

Four-bead model and interactions

Four-bead models have been applied to the study of the folding of a designed three-helix-bundle protein (63), the assembly of a tetrameric α -helical bundle (24, 64), and the aggregation of polyalanines (25, 65, 66). The four-bead model used in this study predicts an α -helix→ β -hairpin transition (32), an important step in fibril formation. In recent studies of $A\beta$ dimer formation, this model predicted several β -strand-rich planar dimer conformations (33). The four-bead model with amino acid-specific interactions due to hydropathy captures general features of the observed *in vitro* oligomerization differences between the two predominant full-length forms of $A\beta$ found *in vivo*, $A\beta1-40$ and $A\beta1-42$ (27).

Geometry of the model protein

In the four-bead model, each amino acid in a protein is modeled by four beads (32)—one bead each for the α -carbon, C_α ; the amide nitrogen, N ; the carbonyl group C' ; and the side-chain atoms, C_β . The exception is Gly, which lacks C_β .

Interactions

A backbone hydrogen bonding interaction is introduced between the C' bead of one and the N bead of another amino acid. Because a hydrogen bond is

directional, auxiliary bonds are introduced to model the angular dependence of the hydrogen bond, as described in detail elsewhere (32). The strength of the backbone hydrogen bonding interaction is ϵ_{HB} .

Amino acid-specific interactions are introduced into the four-bead model according to Urbanc et al. (27). These interactions include an effective hydrophobic attraction (hydrophilic repulsion) between pairs of hydrophobic (hydrophilic) side-chains. The effect of surface area also is considered. An effective hydrophobic attraction is modeled by a single attractive potential well with an interaction range from 3.07Å that is the sum of two hard core radii to 7.5Å.

To better model the complexity of individual side-chains, we define hydropathic interaction strengths here in a different way than as defined in earlier work Urbanc et al. (27). For example, at physiologic pH, the N_ϵ amino group of Lys is positively charged, whereas the *n*-butyl portion of the side-chain is hydrophobic. The interaction scheme described below accounts for interactions among these different parts of the Lys side-chains and hydrophilic or hydrophobic parts of other amino acid side-chains. Interaction strengths between pairs of side-chain beads are defined by considering individual hydropathic strengths and of heavy side-chain atoms (i.e. all atoms except hydrogens) composing the side-chain, as defined in the framework of the united-atom protein model (67).

In addition to the effective hydropathic interactions, we introduce effective electrostatic interactions between two charged amino acids as a “short-range” interaction considering the “screening” effect of polar water molecules. We use a cutoff distance 7.5Å and model it by a double-well potential (60). The interaction between two oppositely-charged amino acids is modeled by an attractive double-well potential, whereas the interaction between two identically-charged amino acids is modeled by a repulsive double-well potential. N- or C-terminal charges are not implemented in this study. The maximal hydrophobic potential energy ϵ_{HP} , which occurs between two isoleucines, is set to 0.15 relative to ϵ_{HB} . Experimental values of electrostatic (ionic bonding) interactions in aqueous solutions are 2-10 kcal/mol, which is of the same order of magnitude as the hydrogen bonding energy (68). Therefore, we set the maximum electrostatic interaction strength, ϵ_{CH} , to 1 relative to ϵ_{HB} .

Energy and time units

We define the unit of energy as the energy of the backbone hydrogen bonding interaction. Time is measured by the number of collisions rather than duration passed between two immediately following collisions. Thus, the simulation time cannot be related directly to real time. However, the thermodynamics as well as the temporal sequence of events is not affected.

Analytical methods

Contact map

Two beads are considered “in contact” if their centers of mass are $<7.5\text{\AA}$ apart. To determine the strength of contact between two amino acids, the number of contacts between all the beads of the two amino acids is counted. The contacts between all the pairs of amino acids are visualized in two dimension as a contact map. The values of the contacts are normalized so that the most frequent is 1.0. To represent contact frequencies visually, the most frequent contact is assigned the color red. Contact frequency then becomes proportional to wavelength, so that the smallest contact frequency is blue (the other extreme of our spectrum).

Heat capacity

The heat capacity has been calculated using the relationship

$$C_v = \frac{\langle E^2 \rangle - \langle E \rangle^2}{k_B T^2} \quad (4)$$

where k_B is the Boltzmann constant, and T is the temperature.

Electrostatic and hydrophobic potential energies

In our implementation of DMD with implicit solvent, potential energies between two beads are pre-defined as a function of distance. For electrostatic potential energy, contributions from all the possible pairs of K and E are summed. For hydrophobic potential energy, all the possible pairs of L, V, F, A, and K are considered.

Average oligomer size

We define two peptides are in an aggregate to form an oligomer if inter-peptide distance of any two beads are within 7.5Å. PROTSVIEW software developed in our group are used to get oligomer sizes for system of sixteen $A\beta_{16-22}$ peptides, then, average of oligomer sizes are calculated at a given time for a trajectory. Finally, average and standard error are calculated for 10 trajectories that have the same set of parameters, but slightly different initial positions and velocities.

Results and Discussion

We explore folding of wild-type $A\beta_{16-22}$ peptide and assembly of sixteen wild-type and Arctic-mutant $A\beta_{16-22}$ peptides initially spatially separated in monomeric conformations with no pre-defined secondary structure. Backbone hydrogen bonding is implemented in all trajectories. For the fibrilization study of wild-type $A\beta_{16-22}$ peptides, we consider three different sets of interaction parameters involving effective hydrophobic and electrostatic interactions: (i) all interactions present ($\epsilon_{HP} = 0.15$, $\epsilon_{CH} = 1$); (ii) no hydrophobic interaction ($\epsilon_{HP} = 0$, $\epsilon_{CH} = 1$); and (iii) no electrostatic interaction ($\epsilon_{HP} = 0.15$, and $\epsilon_{CH} = 0$). The rationale for exploring these three sets of interaction parameters is two-fold: (a) to elucidate the role of hydrophobic and electrostatic interactions in wild-type $A\beta_{16-22}$ fibril formation; and (b) to investigate solvent effects. For the fibrillation study of Arctic-mutant $A\beta_{16-22}$ peptides, we implement all interactions ($\epsilon_{HP} = 0.15$, $\epsilon_{CH} = 1$).

For each set of interaction parameters, 26 temperatures are chosen from the temperature range 0.05–0.30. At each temperature, 10 trajectories, initially characterized by sixteen random-coil-like $A\beta_{16-22}$ monomers with different initial atom positions and velocities, are simulated for 10^7 simulation steps. In total, over 1000 aggregation trajectories are computed and analyzed.

Fibrillization of wild-type $A\beta_{16-22}$ peptides with backbone hydrogen bonding and hydropathic and electrostatic interactions

Single or sixteen wild-type $A\beta_{16-22}$ peptides are placed in a cubic box of side 70 Å using periodic boundary conditions and a temperature range of 0.05–0.30 with an interval of 0.01. We acquire 10 trajectories of 10^7 simulation steps each for each temperature with the backbone hydrogen bonding ($\epsilon_{HB} = 1$), hydropathic ($\epsilon_{HP} = 0.15$), and electrostatic interactions ($\epsilon_{EI} = 1$). The last 5×10^6 simulation steps are used for the calculation of the heat capacity.

To compare the heat capacities of a monomer and a 16-mer on the same scale, we normalize the heat capacity of the 16-mer by the number of peptides to obtain the heat capacity per peptide. Fig. 1 shows the temperature dependence of the heat capacity per peptide for a monomer and a 16-mer, and the average number of backbone hydrogen bonds at the end of the simulation (10^7 steps).

Monomer conformational dynamics

The temperature dependence of monomer heat capacity shows two peaks at temperatures 0.07 and 0.12 [Fig. 1]. In temperature range $T < 0.07$, a monomer forms an α -helix that has the lowest potential energy [Fig. 2(a)], but bent structures also are observed in some trajectories (data not shown). In temperature range between two peaks, $0.07 < T < 0.12$, β -hairpin structures are observed [Figure 2(b)]. In this example, a two-residue hairpin loop is stabilized by two backbone hydrogen bonds (yellow dashed lines) between Leu17 and Phe20. This strong contact is readily apparent in the associated contact map [Fig. 2(f)]. In temperature region $T > 0.12$, a monomer is totally extended [Fig. 2(d)] or forms a large loop-like structure stabilized by a contact between Lys16 and Glu22 side-chain beads [Fig. 2(c)], as confirmed by the contact map [Fig. 2(g)].

Peptide assembly

Simulations with sixteen wild-type $A\beta_{16-22}$ peptides with all interactions (HB, HP, and EI) show that fibril formation takes place in temperature range, $0.12 < T < 0.21$ where monomers mostly fold into large loop-like structures. A typical fibrillar aggregate has multi-layers and antiparallel β -strands within

a layer [Fig. 3(c)]. The averaged intra-contact map at $T = 0.17$ shows the absence of all contacts because each peptide in the fibrillar aggregate is fully stretched and only forms inter-peptide contacts [Fig. 3(g)]. The averaged inter-peptide contact map at $T = 0.17$ shows that an antiparallel orientation between neighboring peptides is dominant [Fig. 3(k)]. Simultaneously, there is a strong inter-peptide contact between the positively-charged Lys16 and the negatively-charged Glu22 due to electrostatic interactions. The temperature range within which a large number of backbone hydrogen bonds occur [Fig. 1] corresponds to that within which fibrillization occurs, as expected.

Figure 4 shows a typical fibril formation process. Initially, sixteen spatially-separated peptides with no pre-defined secondary structure are present [Fig. 4(a)]. At 10^4 simulation steps, some aggregates are formed that contain little β -strands. Individual peptides in the aggregates are stretched or bent [Fig. 4(b)]. At 10^5 simulation steps, an antiparallel layer of four β -strands is observed at the bottom of an aggregate and another β -strand exists in the middle [Fig. 4(c)]. At 2×10^6 simulation steps, a three-layered antiparallel fibrillar aggregate is formed, on top of which a monomer peptide (red) is docked by effective hydrophobic attraction [Fig. 4(d)]. At 4×10^6 simulation steps, a docked monomer (red) that was present at 2×10^6 simulation steps becomes “locked” at the end of the top layer [Fig. 4(e)], in agreement with recent results of Nguyen et al. (54). Until 10^7 simulation step, which is the end of our simulation for this study, the structure of the fibril is conserved [Fig. 4(f)].

We observe two stages of $A\beta_{16-22}$ fibril formation. In stage one, a globular aggregate with little β -strand content is formed. Subsequently, some β -strands form a single layer within the aggregate, followed by the formation of another layer, until extensive hydrogen bonding exists throughout the aggregate. Typically, 3–6 peptides form a layer for the system of sixteen peptides. At the second stage, one or more fibrillar aggregates exist, but not all peptides yet exist within aggregates. At this stage, a “dock-and-lock” fibril emanation mechanism operates (39, 54, 55). The large aggregate in Fig. 4(b) is illustrative of the first stage. The peptide in red is docked to the fibril end in Fig. 4(d) and locked to it in Fig. 4(e). The ability of free peptide monomers to add to existing fibril ends in stage two-type reactions, as opposed to a requirement for formation of an initial β -sheet, explains why seeding accelerates the growth process in experimental systems and in simulations (25).

The first stage of fibril formation requires that aggregates initially lacking β -strand structures can rearrange themselves into conformations allowing

backbone hydrogen bonding. Fig. 5 shows the number of backbone hydrogen bonds and the electrostatic and hydrophobic potential energies of sixteen wild-type $A\beta_{16-22}$ peptides, averaged over 10 trajectories at $T=0.17$, where all of the trajectories form fibrillar aggregates. Electrostatic and hydrophobic potential energies reach constant levels after 4×10^6 simulation steps. However, the number of backbone hydrogen bonds fluctuates from $\sim 19-26$, indicative of a flexibility that persists even when the aggregate becomes fibrillar. This plasticity of backbone hydrogen bonding enables the transition from amorphous aggregate to fibril, demonstrating the importance of backbone hydrogen bonds in folding and aggregation, as suggested by Rose et al. (69).

In temperature range $T < 0.12$ or $T > 0.21$, fibril formation is not observed. In temperature range $0.21 < T < 0.28$, amorphous aggregates are found [Figs. 3(d,h,l)]. Hence, the large peak in the heat capacity per peptide of 16-mer at $T=0.21$ [Fig. 1] illustrates the high cost of energy in the conformational change from a fibrillar structure to an amorphous aggregate, which is associated with hydrogen bond disruption. In temperature range $T > 0.28$, no aggregates are formed because thermal fluctuations are too large to allow aggregation (data not shown). The smaller peak in the heat capacity per peptide of 16-mer at $T=0.28$ corresponds to a conformational changes from an aggregated to a disaggregated state [Fig. 1]. The aggregates in temperature range $0.07 < T < 0.12$ have significant amount of β -strand structure [Fig. 3(b)]. The aggregates in temperature range $T < 0.07$ are characterized by a bent intra-peptide structure stabilized by a strong contact between Leu17 and Phe20, but with no significant α -helical or β -strand structure [Figs. 3(a,e)].

Fibrillization of wild-type $A\beta_{16-22}$ peptides with no hydrophobic or electrostatic interactions

The heat capacities of a 16-mer as a function of temperature with either no hydrophobic (HP), no electrostatic (EI), and with HB, HP, and EI is shown in Fig. 6. The predominant peak at $T=0.21$ with all interactions, which corresponds to the conformational change from a fibrillar to an amorphous aggregate, has been shifted to lower temperature. For the trajectories with no HP, some show β -strand formation but none produce multi-layered fibrillar aggregates. However, all trajectories with no EI show formation of fibrillar

aggregates in temperature range $0.13 < T < 0.17$, on the left side of the predominant peak at $T=0.21$. Fig. 7(a) shows a typical conformations with no HP, and Fig. 7(b) with no EI at temperature 0.15.

For fibrillar aggregates formed in the absence of EI, but in the presence of HB and HP, both parallel and antiparallel β -sheet structures are observed, in agreement with findings of Favrin et al. (48). Taken together with the result that antiparallel β -sheet structures were observed in the presence of EI, HB and HP, we conclude that EI strongly favors the antiparallel orientation of the β -sheet in the fibrillar aggregate. The antiparallel fibril structure is associated with salt bridge formation between Lys16 and Glu22. In the absence of HP, but with HB and EI present, only antiparallel β -strands are observed. This result also supports the importance of EI in antiparallel β -sheet formation during fibrillization, in agreement with Klimov and Thirumalai (45). We do not observe both parallel and antiparallel β -sheet with HB, HP and EI, as do Meinke and Hansmann (53), because the antiparallel β -sheets have lower energy in our model than do the parallel β -sheets and the system reaches the lower energy state after 10^7 simulation steps in all trajectories.

Fibrillization of Arctic-mutant (E22G) $A\beta_{16-22}$ peptides

A typical fibril of Arctic-mutant $A\beta_{16-22}$ peptides [Fig. 7(c)] has parallel and antiparallel β -strands as the fibril with no EI [Figs. 7(b)]. The reason why we observe parallel β -strands is due to decreased role of electrostatic interaction in fibrillization of Arctic-mutant $A\beta_{16-22}$ peptides since negatively charged Glu is mutated as a non-charged Gly, therefore the peptide has only one positively charged residue, K16. The similarity between Arctic-mutant $A\beta_{16-22}$ and wild-type $A\beta_{16-22}$ with no EI is also shown in heat capacity for having the similar heat capacities at the temperatures lower than 0.18, and another bump at $T = 0.2$ for Arctic, and at $T = 0.21$ for no EI [Fig. 6].

As for the kinetics of aggregation, we observe that initially well-separated single peptides oligomerize, then fibrillize. Oligomerization usually happens within 2×10^5 simulation steps, while fibrillization takes 2×10^6 simulation steps. To find out wild-type or Arctic-mutant $A\beta_{16-22}$ peptides aggregate faster, we analyze the time progression of average oligomer sizes, which is shown in Fig. 8(a) for temperature 0.15. At 3×10^4 step, sixteen wild-type $A\beta_{16-22}$ peptides aggregate forming 16-mer in all of the 10 trajectories, while the average oligomer size of Arctic-mutant $A\beta_{16-22}$ peptides is 7. Therefore, we conclude that wild-type $A\beta_{16-22}$ peptides oligomerize faster than Arctic-

mutant $A\beta_{16-22}$, which is true for other temperatures 0.13, 0.14, and 0.16 (data not shown). This result is consistent with the atomic force microscopy image by Cheng et al. (13) in which wild-type $A\beta_{1-42}$ oligomers are more abundant than Arctic-mutant $A\beta_{1-42}$ oligomers at 3 minute. Electrostatic potential energy of Arctic-mutant $A\beta_{16-22}$ peptides is close to zero during oligomerization [Fig. 8(b)], which suggests that the negligible role of electrostatic interaction in driving oligomerization is responsible for slower oligomerization of Arctic-mutant $A\beta_{16-22}$ peptides. It implies that oligomerization is not simply hydrophobic driven, rather electrostatic interaction takes part in oligomerization cooperatively.

To compare wild-type or Arctic-mutant $A\beta_{16-22}$ peptides fibrillize faster quantitatively, we plot how many residues per peptide are assigned as β -strand as a function of simulation step. Fig. 9 shows that, at 1×10^6 simulation step, number of β -strand residues per peptide reaches the final value for Arctic-mutant $A\beta_{16-22}$ peptides, but not for wild-type at temperature 0.15. Therefore, we conclude that Arctic-mutant $A\beta_{16-22}$ peptides fibrillize faster than wild-type $A\beta_{16-22}$ peptides, which is consistent with many experimental results (13, 15–18). Faster fibrillization of Arctic-mutant $A\beta_{16-22}$ peptides is also observed at temperatures 0.13, 0.14, and 0.16 (data not shown). For the reason why Arctic-mutant (E22G) $A\beta_{16-22}$ peptides fibrillize faster than wild-type, smaller volume, better flexibility, and no charge of G22 residue allow better plasticity required for fibrillization, and also enable the rearrangement of aggregated peptides easier than in wild-type.

Conclusion

Implementation of an *ab initio* DMD procedure incorporating a modified four-bead peptide model enabled us to visualize aggregation of $A\beta_{16-22}$ peptides from spatially-separated random coil-like peptides into structured, fibril-like units. These units consist of stacked β -sheets, a result consistent with the common cross- β core structures determined for amyloid fibrils in X-ray diffraction studies (70, 71) and previous simulation work (44, 45, 48, 49, 54, 55). Within each β -sheet, the peptides are in an antiparallel arrangement, which is consistent with solid-state NMR results for $A\beta_{16-22}$ fibrils at pH 7.4 (38, 41, 72). The fibril formation for wild-type $A\beta_{16-22}$ peptides occurs in temperature range $0.12 < T < 0.21$, in which a single wild-type $A\beta_{16-22}$ peptide folds as a loop-like structure. Two stages of fibril formation

are observed. First, monomers assemble into an amorphous aggregate, followed by emergence of β -strand structure, first within one layer. Hydrogen bonding then is perpetuated through the aggregate to produce a fibril-like structure. At this stage, flexibility of the peptide backbone is required to form the backbone hydrogen bonds, as demonstrated by large fluctuations in backbone hydrogen bond number. In a second stage, free monomers “dock” with, and then “lock” into the preformed fibril, in agreement with experimental findings by Esler et al. (39) and simulation results by Nguyen et al. (54), Takeda and Klimov (55). The locking step occurs after the first stage is complete because this later stage requires a preformed fibril. The simulation with no EI, but with HB and HP, produces fibrils containing parallel or antiparallel β -sheets. In contrast, simulations with no HP, but with HB and EI, do not produce ordered fibrillar aggregates, but rather more diffuse aggregates with some β -strand structure. These latter results should be testable experimentally by studying $A\beta_{16-22}$ fibril formation at low pH using an apolar solvent that would provide a strongly hydrophobic environment.

We find two peaks in our calculated heat capacity under the conditions where all three interactions (HB, HP, and EI) exist. The peak at lower temperature represents a conformational change from a fibrillar to an amorphous aggregate. The peak at higher temperature represents a conformational transition from an aggregated into a disaggregated state. When simulated in the absence of EI or HP, the higher temperature peak disappears, a feature that is particularly evident in the case of simulations without HP interactions. Differential scanning calorimetry was used to investigate thermal transitions of type I collagen fibrils and the melting curves displayed two pronounced heat absorption peaks (73), consistent with this supposition. Additional experiments at low pH, as well as in apolar solvents, would provide further *in vitro* testing of this notion.

Simulation of Arctic-mutant $A\beta_{16-22}$ peptides show that their fibrillar structure contains parallel and antiparallel β -strands, which resembles the fibrillar structure of wild-type $A\beta_{16-22}$ peptides with no EI. Comparison of aggregation kinetics shows that Arctic-mutant $A\beta_{16-22}$ peptides oligomerize slower, but fibrillize faster than wild-type $A\beta_{16-22}$ peptides with all three interactions (HB, HP, and EI). Slower oligomerization of Arctic-mutant $A\beta_{16-22}$ peptides is due to negligible role of electrostatic interaction because of G22, while faster fibrillization is due to smaller volume, better flexibility, and no charge of G22 residue which allow better flexibility and ease of rearrangement that are required for fibrillization.

Acknowledgments

We thank J. M. Borreguero, F. Ding and N. V. Dokholyan for the implementation of the four-bead protein model, G. Paul for the DMD code optimization, and G. Bitan, N. Lazo, and S. Maji for helpful discussions. We acknowledge the NIH, Memory Ride Foundation, Zenith Foundation, Petroleum Research Foundation, and Stephen Bechtel, Jr. for financial support to Boston University and NIH grant AG027818 to UCLA.

References

- [1] Taylor, J. P., J. Hardy, and K. H. Fischbeck, 2002. Toxic proteins in neurodegenerative disease. *Science*. 296:1991–1995.
- [2] Selkoe, D. J., 1991. The molecular pathology of Alzheimer’s disease. *Neuron*. 6:487–498.
- [3] Hardy, J., and D. J. Selkoe, 2002. The amyloid hypothesis of Alzheimer’s disease: progress and problems on the road to therapeutics. *Science*. 297:353–356.
- [4] Alzheimer, A., 1906. Über einen eigenartigen schweren Erkrankungsprozeß der Hirnrinde. *Neurologisches Centralblatt*. 23:1129–1136.
- [5] Selkoe, D. J., 2001. Alzheimer’s disease: Genes, proteins, and therapy. *Physiol. Rev.* 81:741–766.
- [6] Lambert, M. P., A. K. Barlow, B. A. Chromy, C. Edwards, R. Freed, M. Liosatos, T. E. Morgan, I. Rozovsky, B. Trommer, K. L. Viola, P. Wals, C. Zhang, C. E. Finch, G. A. Krafft, and W. L. Klein, 1998. Diffusible, nonfibrillar ligands derived from $A\beta_{1-42}$ are potent central nervous system neurotoxins. *Proc. Natl. Acad. Sci. USA*. 95:6448–6453.
- [7] Walsh, D. M., D. M. Hartley, Y. Kusumoto, Y. Fezoui, M. M. Condron, A. Lomakin, G. B. Benedek, D. J. Selkoe, and D. B. Teplow, 1999.

- Amyloid β -protein fibrillogenesis. Structure and biological activity of protofibrillar intermediates. *J. Biol. Chem.* 274:25945–25952.
- [8] Klein, W. L., G. A. Krafft, and C. E. Finch, 2001. Targeting small $A\beta$ oligomers: the solution to an Alzheimer's disease conundrum? *Trends Neurosci.* 24:219–224.
 - [9] Klein, W. L., W. B. Stine, and D. B. Teplow, 2004. Small assemblies of unmodified amyloid β -protein are the proximate neurotoxin in Alzheimer's disease. *Neurobiol. Aging.* 25:569–580.
 - [10] Kirkkitadze, M. D., G. Bitan, and D. B. Teplow, 2002. Paradigm shifts in Alzheimer's disease and other neurodegenerative disorders: the emerging role of oligomeric assemblies. *J. Neurosci. Res.* 69:567–577.
 - [11] Roher, A. E., J. Baudry, M. O. Chaney, Y. M. Kuo, W. B. Stine, and M. R. Emmerling, 2000. Oligomerizaiton and fibril asssembly of the amyloid- β protein. *Biochim. Biophys. Acta.* 1502:31–43.
 - [12] Rottkamp, C. A., C. S. Atwood, J. A. Joseph, A. Nunomura, G. Perry, and M. A. Smith, 2002. The state versus amyloid- β : the trial of the most wanted criminal in Alzheimer disease. *Peptides.* 23:1333–1341.
 - [13] Cheng, I. H., K. Scearce-Levie, J. Legleiter, J. J. Palop, H. Gerstein, N. Bien-Ly, J. Puolivali, S. Lesne, K. H. Ashe, P. J. Muchowski, and L. Mucke, 2007. Accelerating amyloid- β fibrillization reduces oligomer levels and functional deficits in Alzheimer disease mouse models. *J Biol Chem* 282:23818–23828.
 - [14] Nilsberth, C., A. Westlind-Danielsson, C. B. Eckman, M. M. Condron, K. Axelman, C. Forsell, C. Stenh, J. Luthman, D. B. Teplow, S. G. Younkin, J. Näslund, and L. Lannfelt, 2001. The ‘Arctic’ APP mutation (E693G) causes Alzheimer's disease by enhanced $A\beta$ protofibril formation. *Nat. Neurosci.* 4:887–893.
 - [15] Murakami, K., K. Irie, A. Morimoto, H. Ohigashi, M. Shindo, M. Nagao, T. Shimizu, and T. Shirasawa, 2002. Synthesis, aggregation, neurotoxicity, and secondary structure of various $A\beta$ 1-42 mutants of familial Alzheimer's disease at positions 21-23. *Biochem Biophys Res Commun* 294:5–10.

- [16] Lashuel, H. A., D. M. Hartley, B. M. Petre, J. S. Wall, M. N. Simon, T. Walz, and P. T. J. Lansbury, 2003. Mixtures of wild-type and a pathogenic (E22G) form of A β 40 *in vitro* accumulate protofibrils, including amyloid pores. *J Mol Biol* 332:795–808.
- [17] Johansson, A.-S., F. Berglind-Dehlin, G. Karlsson, K. Edwards, P. Gellerfors, and L. Lannfelt, 2006. Physiochemical characterization of the Alzheimer's disease-related peptides A β 1-42Arctic and A β 1-42wt. *FEBS J* 273:2618–30.
- [18] Hori, Y., T. Hashimoto, Y. Wakutani, K. Urakami, K. Nakashima, M. M. Condron, S. Tsubuki, T. C. Saido, D. B. Teplow, and T. Iwatsubo, 2007. The Tottori (D7N) and English (H6R) familial Alzheimer disease mutations accelerate A β fibril formation without increasing protofibril formation. *J Biol Chem* 282:4916–23.
- [19] Teplow, D. B., N. D. Lazo, G. Bitan, S. Bernstein, T. Wyttenbach, M. T. Bowers, A. Baumketner, J.-E. Shea, B. Urbanc, L. Cruz, J. Borreguero, and H. E. Stanley, 2006. Elucidating amyloid β -protein folding and assembly: A multidisciplinary approach. *Acc. Chem. Res.* 39:635–645.
- [20] Shakhnovich, E. I., 1996. Modeling protein folding: the beauty and power of simplicity. *Fold. Des.* 1:R50–R54.
- [21] Derreumaux, P., and N. Mousseau, 2007. Coarse-grained protein molecular dynamics simulations. *J Chem Phys* 126:025101.
- [22] Zhou, Y. Q., and M. Karplus, 1997. Folding thermodynamics of a model three-helix-bundle protein. *Proc. Natl. Acad. Sci. USA*. 94:14429–14432.
- [23] Dokholyan, N. V., S. V. Buldyrev, H. E. Stanley, and E. I. Shakhnovich, 1998. Discrete molecular dynamics studies of the folding of a protein-like model. *Fold. Des.* 3:577–587.
- [24] Smith, A. V., and C. K. Hall, 2001. Assembly of a tetrameric α -helical bundle: computer simulations on an intermediate-resolution protein model. *Proteins: Struct. Func. & Genet.* 44:376–391.
- [25] Nguyen, H. D., and C. K. Hall, 2004. Molecular dynamics simulations of spontaneous fibril formation by random-coil peptides. *Proc. Natl. Acad. Sci. USA*. 101:16180–16185.

- [26] Ding, F., N. V. Dokholyan, S. V. Buldyrev, H. E. Stanley, and E. I. Shakhnovich, 2002. Direct molecular dynamics observation of protein folding transition state ensemble. *Biophys. J.* 83:3525–3532.
- [27] Urbanc, B., L. Cruz, S. Yun, S. V. Buldyrev, G. Bitan, D. B. Teplow, and H. E. Stanley, 2004. *In silico* study of amyloid β -protein folding and oligomerization. *Proc. Natl. Acad. Sci. USA.* 101:17345–17350.
- [28] Yun, S., B. Urbanc, L. Cruz, G. Bitan, D. B. Teplow, and H. E. Stanley, 2007. Role of electrostatic interactions in amyloid β -protein ($A\beta$) oligomer formation: a discrete molecular dynamics study. *Biophys J* 92:4064–77.
- [29] Ding, F., N. V. Dokholyan, S. V. Buldyrev, H. E. Stanley, and E. I. Shakhnovich, 2002. Molecular dynamics simulation of the SH3 domain aggregation suggests a generic amyloidogenesis mechanism. *J. Mol. Biol.* 324:851–857.
- [30] Borreguero, J. M., N. V. Dokholyan, S. V. Buldyrev, E. I. Shakhnovich, and H. E. Stanley, 2002. Thermodynamics and folding kinetics analysis of the SH3 domain from discrete molecular dynamics. *J. Mol. Biol.* 318:863–876.
- [31] Peng, S., F. Ding, B. Urbanc, S. V. Buldyrev, L. Cruz, H. E. Stanley, and N. V. Dokholyan, 2004. Discrete molecular dynamics simulations of peptide aggregation. *Phys. Rev. E* 69:041908.
- [32] Ding, F., J. M. Borreguero, S. V. Buldyrey, H. E. Stanley, and N. V. Dokholyan, 2003. Mechanism for the α -helix to β -hairpin transition. *Proteins: Struct. Func. & Genet.* 53:220–228.
- [33] Urbanc, B., L. Cruz, F. Ding, D. Sammond, S. Khare, S. V. Buldyrev, H. E. Stanley, and N. V. Dokholyan, 2004. Molecular dynamics simulation of amyloid β dimer formation. *Biophys. J.* 87:2310–2321.
- [34] Ding, F., S. V. Buldyrev, and N. V. Dokholyan, 2005. Folding Trp-cage to NMR resolution native structure using a coarse-grained model. *Biophys. J.* 88:147–155.
- [35] Borreguero, J. M., B. Urbanc, N. D. Lazo, S. V. Buldyrev, D. B. Teplow, and H. E. Stanley, 2005. Folding events in the 21-30 region of amyloid

- β -protein ($A\beta$) studied *in silico*. *Proc. Natl. Acad. Sci. USA.* 102:6015–6020.
- [36] Esler, W. P., E. R. Stimson, J. R. Ghilardi, Y. A. Lu, A. M. Felix, H. V. Vinters, P. W. Mantyh, J. P. Lee, and J. E. Maggio, 1996. Point substitution in the central hydrophobic cluster of a human β -amyloid congener disrupts peptide folding and abolishes plaque competence. *Biochemistry*. 35:13914–13921. <http://dx.doi.org/10.1021/bi961302+>.
 - [37] Lynn, D. G., and S. C. Meredith, 2000. Review: model peptides and the physicochemical approach to β -amyloids. *J. Struct. Biol.* 130:153–173.
 - [38] Balbach, J. J., Y. Ishii, O. N. Antzutkin, R. D. Leapman, N. W. Rizzo, F. Dyda, J. Reed, and R. Tycko, 2000. Amyloid fibril formation by $A\beta_{16-22}$, a seven-residue fragment of the Alzheimer's β -amyloid peptide, and structural characterization by solid state NMR. *Biochemistry*. 39:13748–13759.
 - [39] Esler, W. P., E. R. Stimson, J. M. Jennings, H. V. Vinters, J. R. Ghilardi, J. P. Lee, P. W. Mantyh, and J. E. Maggio, 2000. Alzheimer's disease amyloid propagation by a template-dependent dock-lock mechanism. *Biochemistry* 39:6288–95.
 - [40] Gordon, D. J., K. L. Sciarretta, and S. C. Meredith, 2001. Inhibition of β -amyloid(40) fibrillogenesis and disassembly of β -amyloid(40) fibrils by short β -amyloid congeners containing N-methyl amino acids at alternate residues. *Biochemistry* 40:8237–8245.
 - [41] Petkova, A. T., G. Bunkowsky, F. Dyda, R. D. Leapman, W.-M. Yau, and R. Tycko, 2004. Solid state NMR reveals a pH-dependent antiparallel β -sheet registry in fibrils formed by a β -amyloid peptide. *J. Mol. Biol.* 335:247–260.
 - [42] Gordon, D. J., J. J. Balbach, R. Tycko, and S. C. Meredith, 2004. Increasing the amphiphilicity of an amyloidogenic peptide changes the β -sheet structure in the fibrils from antiparallel to parallel. *Biophys. J.* 86:428–434.
 - [43] Petty, S. A., and S. M. Decatur, 2005. Experimental evidence for the reorganization of β -strands within aggregates of the $A\beta(16-22)$ peptide. *J Am Chem Soc* 127:13488–9.

- [44] Ma, B., and R. Nussinov, 2002. Stabilities and conformations of Alzheimer's β -amyloid peptide oligomers ($A\beta_{16-22}$, $A\beta_{16-35}$, and $A\beta_{10-35}$): sequence effects. *Proc. Natl. Acad. Sci. USA.* 99:14126–14131.
- [45] Klimov, D. K., and D. Thirumalai, 2003. Dissecting the assembly of $A\beta_{16-22}$ amyloid peptides into antiparallel β sheets. *Structure.* 11:295–307.
- [46] Klimov, D. K., J. E. Straub, and D. Thirumalai, 2004. Aqueous urea solution destabilizes $A\beta(16-22)$ oligomers. *Proc. Natl. Acad. Sci. USA.* 101:14760–14765. <http://dx.doi.org/10.1073/pnas.0404570101>.
- [47] Hwang, W., S. Zhang, R. D. Kamm, and M. Karplus, 2004. Kinetic control of dimer structure formation in amyloid fibrillogenesis. *Proc. Natl. Acad. Sci. USA.* 101:12916–12921.
- [48] Favrin, G., A. Irbäck, and S. Mohanty, 2004. Oligomerization of amyloid $A\beta_{16-22}$ peptides using hydrogen bonds and hydrophobicity forces. *Biophys. J.* 87:3657–3664. <http://dx.doi.org/10.1529/biophysj.104.046839>.
- [49] Santini, S., N. Mousseau, and P. Derreumaux, 2004. In silico assembly of Alzheimer's $A\beta16-22$ peptide into β -sheets. *J. Am. Chem. Soc.* 126:11509–11516. <http://dx.doi.org/10.1021/ja047286i>.
- [50] Santini, S., G. Wei, N. Mousseau, and P. Derreumaux, 2004. Pathway complexity of Alzheimer's β -amyloid $A\beta16-22$ peptide assembly. *Structure* 12:1245–1255. <http://dx.doi.org/10.1016/j.str.2004.04.018>.
- [51] Gnanakaran, S., R. Nussinov, and A. E. García, 2006. Atomic-level description of amyloid β -dimer formation. *J. Am. Chem. Soc.* 128:2158–2159. <http://dx.doi.org/10.1021/ja0548337>.
- [52] Rohrig, U. F., A. Laio, N. Tantalo, M. Parrinello, and R. Petronzio, 2006. Stability and structure of oligomers of the Alzheimer peptide $A\beta_{16-22}$: from the dimer to the 32-mer. *Biophys J* 91:3217–29.
- [53] Meinke, J. H., and U. H. E. Hansmann, 2007. Aggregation of β -amyloid fragments. *J Chem Phys* 126:014706.

- [54] Nguyen, P. H., M. S. Li, G. Stock, J. E. Straub, and D. Thirumalai, 2007. Monomer adds to preformed structured oligomers of A β -peptides by a two-stage dock-lock mechanism. *Proc Natl Acad Sci U S A* 104:111–6.
- [55] Takeda, T., and D. K. Klimov, 2007. Dissociation of A β_{16-22} amyloid fibrils probed by molecular dynamics. *J Mol Biol* 368:1202–13.
- [56] Cheon, M., I. Chang, S. Mohanty, L. M. Luheshi, C. M. Dobson, M. Vendruscolo, and G. Favrin, 2007. Structural reorganisation and potential toxicity of oligomeric species formed during the assembly of amyloid fibrils. *PLoS Comput Biol* 3:1727–1738.
- [57] Sawaya, M. R., S. Sambashivan, R. Nelson, M. I. Ivanova, S. A. Sievers, M. I. Apostol, M. J. Thompson, M. Balbirnie, J. J. W. Wiltzius, H. T. McFarlane, A. O. Madsen, C. Riek, and D. Eisenberg, 2007. Atomic structures of amyloid cross- β spines reveal varied steric zippers. *Nature* 447:453–7.
- [58] Zheng, J., B. Ma, and R. Nussinov, 2006. Consensus features in amyloid fibrils: sheet-sheet recognition via a (polar or nonpolar) zipper structure. *Phys Biol* 3:P1–4.
- [59] Urbanc, B., L. Cruz, D. B. Teplow, and H. E. Stanley, 2006. Computer simulations of Alzheimer's amyloid β -protein folding and assembly. *Curr Alzheimer Res* 3:493–504.
- [60] Urbanc, B., J. Borreguero, L. Cruz, and H. E. Stanley, 2006. *Ab initio* discrete molecular dynamics approach to protein folding and aggregation. *Methods Enzymol.* 412:314–338.
- [61] Rapaport, D. C., 1997. The art of molecular dynamics simulation. Cambridge University Press, Cambridge.
- [62] Berendsen, H. J. C., J. Postma, W. V. Gunsteren, A. DiNola, and J. Haak, 1984. Molecular dynamics with coupling to an external bath. *J. Chem. Phys.* 81:3684–3690.
- [63] Takada, S., Z. Luthey-Schulten, and P. G. Wolynes, 1999. Folding dynamics with nonadditive forces: A simulation study of a designed helical protein and a random heteropolymer. *J. Chem. Phys.* 110:11616–11629.

- [64] Smith, A. V., and C. K. Hall, 2001. Protein refolding versus aggregation: Computer simulations on an intermediate-resolution protein model. *J. Mol. Biol.* 312:187–202.
- [65] Nguyen, H. D., and C. K. Hall, 2004. Phase diagrams describing fibrillization by polyalanine peptides. *Biophys. J.* 87:4122–4134. <http://dx.doi.org/10.1529/biophysj.104.047159>.
- [66] Nguyen, H. D., and C. K. Hall, 2005. Kinetics of fibril formation by polyalanine peptides. *J. Biol. Chem.* 280:9074–9082. <http://dx.doi.org/10.1074/jbc.M407338200>.
- [67] Borreguero, J. M., 2004. Computational studies of protein stability and folding kinetics. Ph.D. thesis, Boston University, USA.
- [68] Creighton, T., 1993. Proteins: structures and molecular properties, second edition. W. H. Freeman and Co., New York.
- [69] Rose, G. D., P. J. Fleming, J. R. Banavar, and A. Maritan, 2006. A backbone-based theory of protein folding. *Proc Natl Acad Sci U S A* 103:16623–33.
- [70] Eanes, E. D., and G. G. Glenner, 1968. X-ray diffraction studies on amyloid filaments. *J. Histochem. Cytochem.* 16:673–677.
- [71] Sunde, M., L. C. Serpell, M. Bartlam, P. E. Fraser, M. B. Pepys, and C. C. Blake, 1997. Common core structure of amyloid fibrils by synchrotron X-ray diffraction. *J. Mol. Biol.* 273:729–739.
- [72] Tycko, R., and Y. Ishii, 2003. Constraints on supramolecular structure in amyloid fibrils from two-dimensional solid-state NMR spectroscopy with uniform isotopic labeling. *J. Am. Chem. Soc.* 125:6606–6607.
- [73] Tiktopulo, E. I., and A. V. Kajava, 1998. Denaturation of type I collagen fibrils is an endothermic process accompanied by a noticeable change in the partial heat capacity. *Biochemistry.* 37:8147–52. <http://dx.doi.org/10.1021/bi980360n>.
- [74] Frishman, D., and P. Argos, 1995. Knowledge-based protein secondary structure assignment. *Proteins: Struct. Func. & Genet.* 23:566–579.

- [75] Humphrey, W., A. Dalke, and K. Schulten, 1996. VMD: visual molecular dynamics. *J. Mol. Graph.* 14:33–38.

Figure captions:

Figure 1: Temperature dependence of heat capacity per peptide and number of backbone hydrogen bonds for a monomer and a 16-mer of wild-type A β_{16-22} peptides. The left y-axis shows heat capacity per peptide for a monomer (black) and a 16-mer (red), and the right y-axis shows the number of hydrogen bonds for 16-mer (blue). Each value is the average over 10 trajectories. Error bar denotes standard error between trajectories. STRIDE software in the VMD package (74) is used to calculate the number of backbone hydrogen bonds with a distance cutoff of 3.0Å and an angle cutoff of 20°.

Figure 2: Representative conformations and averaged contact maps for a single wild-type A β_{16-22} peptide at 10^7 simulation steps. Temperatures at (a,e) 0.05, (b,f) 0.11 , (c,g) 0.17 , and (d,h) 0.24 . Lys is denoted in blue, and Glu in red, and other residues in white in (a-d). Ball shows C β atom, and stick shows the backbone of a peptide. Hydrogen bonds are denoted with yellow dashed lines in (b). The strength of the contact map is color-coded following the rainbow scheme: from blue (no contact) to red (the largest number of contacts). Each contact map is an average over 10 trajectories. The structural conformations are generated by the VMD package (75).

Figure 3: Representative conformations and averaged (e-h) intra- and (i-l) inter- contact maps for 16-mer of wild-type A β_{16-22} peptides at 10^7 simulation steps. Temperatures at (a,e,i) 0.05, (b,f,j) 0.11, (c,g,k) 0.17 , and (d,h,l) 0.24. β -strand is denoted in a yellow arrow for (a-d). Color coding for contact maps is same as in Fig. 2.

Figure 4: Time progression of sixteen wild-type A β_{16-22} peptides. Simulation step at (a) 0, (b) 10^4 , (c) 10^5 , (d) 2×10^6 , (e) 4×10^6 , and (f) 10^7 . β -strand is denoted in a yellow arrow. The peptide shown in red in (d) and (e) is the same one. Temperature is at 0.17.

Figure 5: Potential energies and number of hydrogen bonds for sixteen wild-type A β_{16-22} peptides. Electrostatic potential energy (black), hydrophobic potential energy (red), and number of hydrogen bonds (blue). Each value is the average over 10 trajectories. Error bar denotes standard error between trajectories. Temperature is at 0.17.

Figure 6: Temperature dependence of heat capacity for sixteen wild-type and Arctic-mutant $\text{A}\beta_{16-22}$ peptides. For wild-type, interactions are controlled, (i) with hydrogen bonding, hydrophobic, electrostatic interactions (black), (ii) no hydrophobic interaction (green), (iii) no electrostatic interaction (blue). Heat capacity for Arctic-mutant is shown in red. Error bar denotes standard error between trajectories.

Figure 7: Representative conformations of 16-mer. Representative conformations with (a) no hydrophobic (No HP), (b) no electrostatic interaction (No EI) for wild-type, and (c) for Arctic-mutant $\text{A}\beta_{16-22}$ peptides. Temperature is at 0.15.

Figure 8: Time progression of average oligomer size and potential energies for sixteen wild-type and Arctic-mutant $\text{A}\beta_{16-22}$ peptides during early aggregation. Each value is the average over 10 trajectories. Error bar denotes standard error between trajectories. For (a) average oligomer size, wild-type is denoted in black, and Arctic-mutant in red. For (b) average potential energies, electrostatic potential energy (PE) is denoted in black, hydrophobic PE in blue for wild-type. For Arctic-mutants, electrostatic PE is in maroon, hydrophobic PE in red. Temperature is at 0.15.

Figure 9: Time progression of number of residues per peptide assigned as β -strand for sixteen wild-type and Arctic-mutant $\text{A}\beta_{16-22}$ peptides. Wild-type is denoted in black, and Arctic-mutant in red. Temperature is at 0.15. Secondary structure assignment is done by STRIDE software in the VMD package (74). Error bar denotes standard error between trajectories.

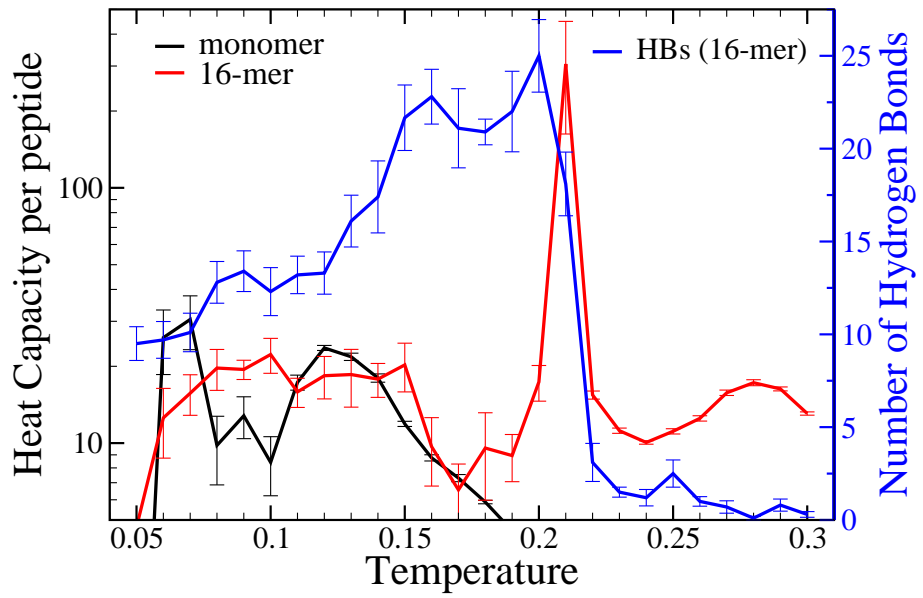


Figure 1:

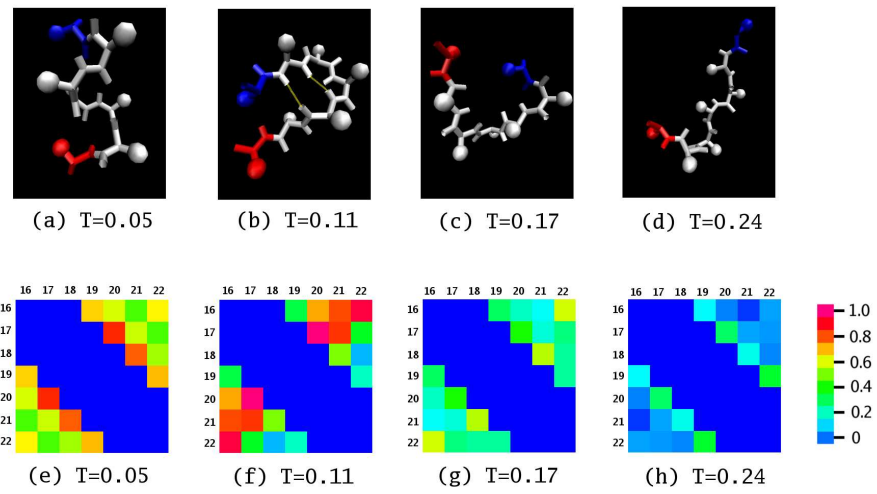


Figure 2:

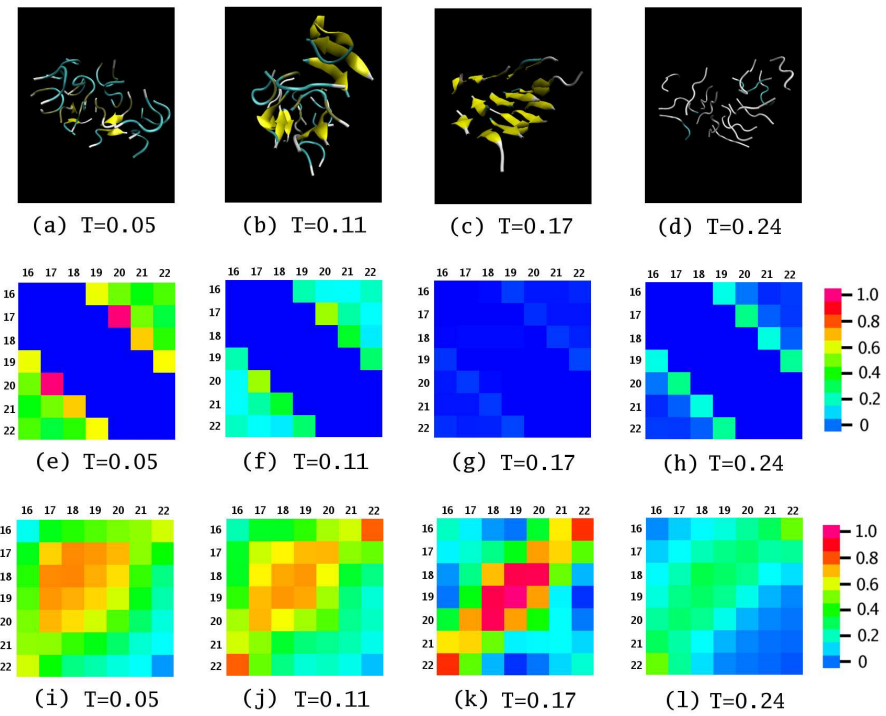


Figure 3:

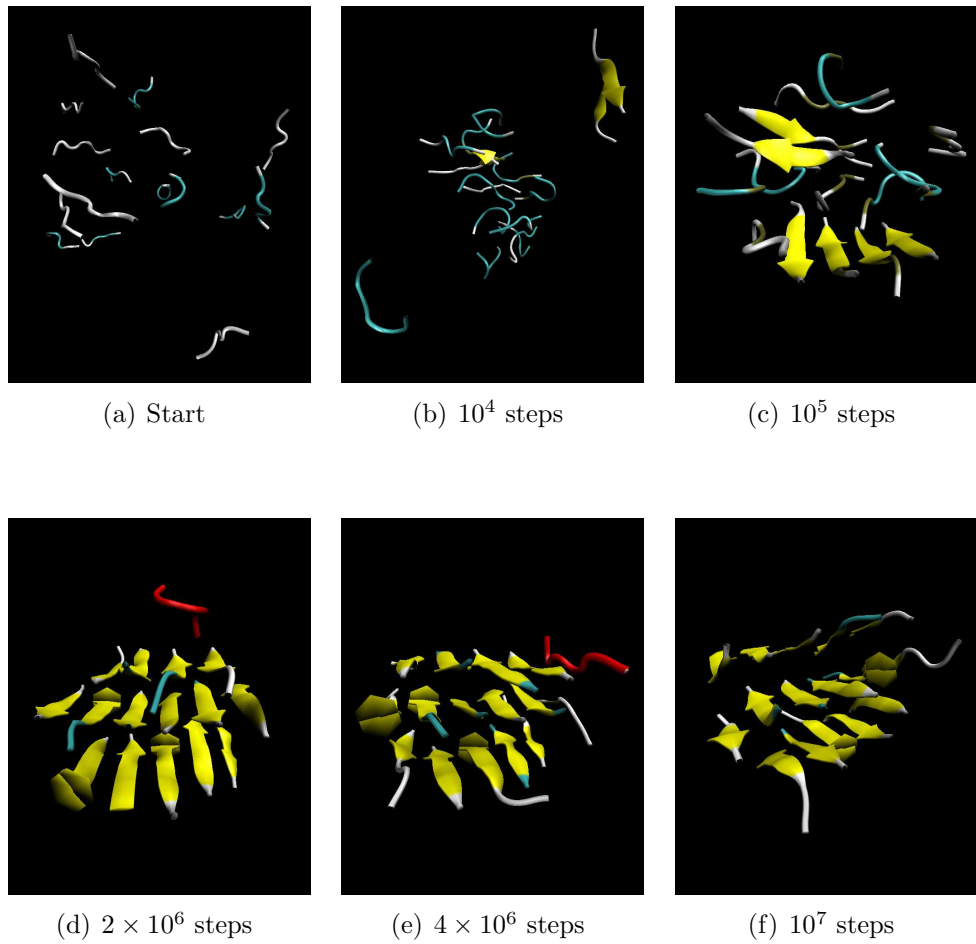


Figure 4:

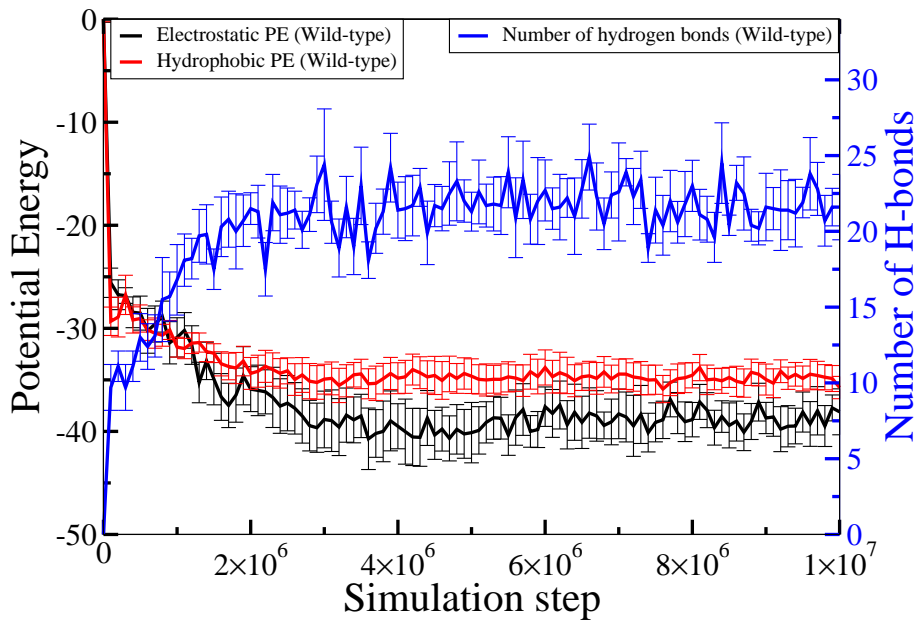


Figure 5:

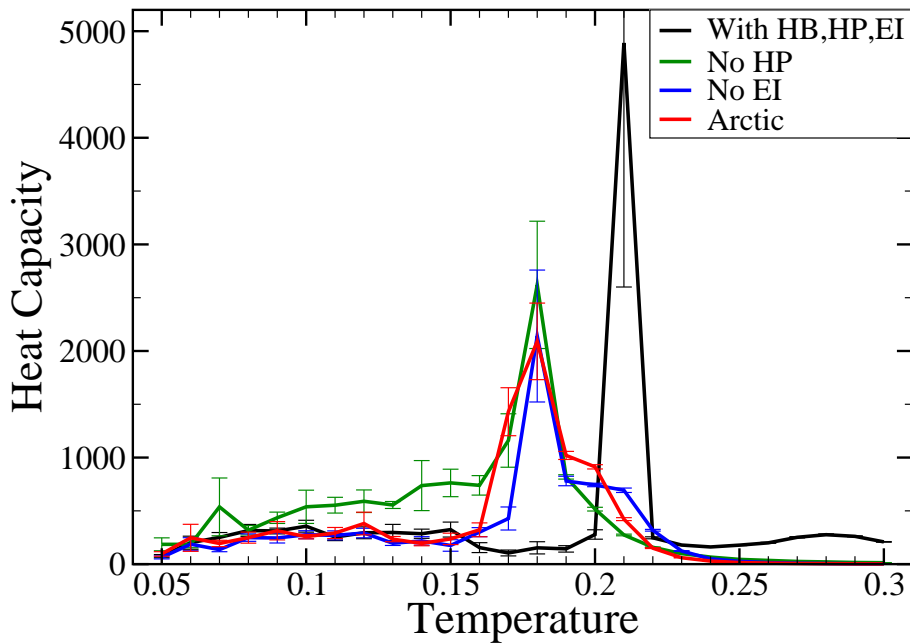
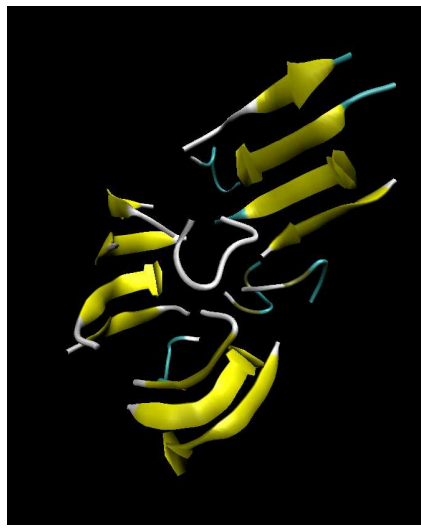
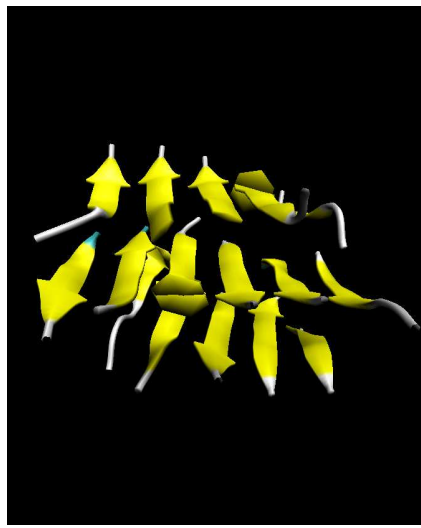


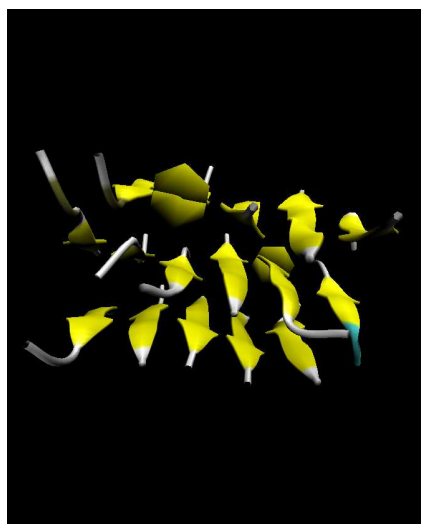
Figure 6:



(a) No HP

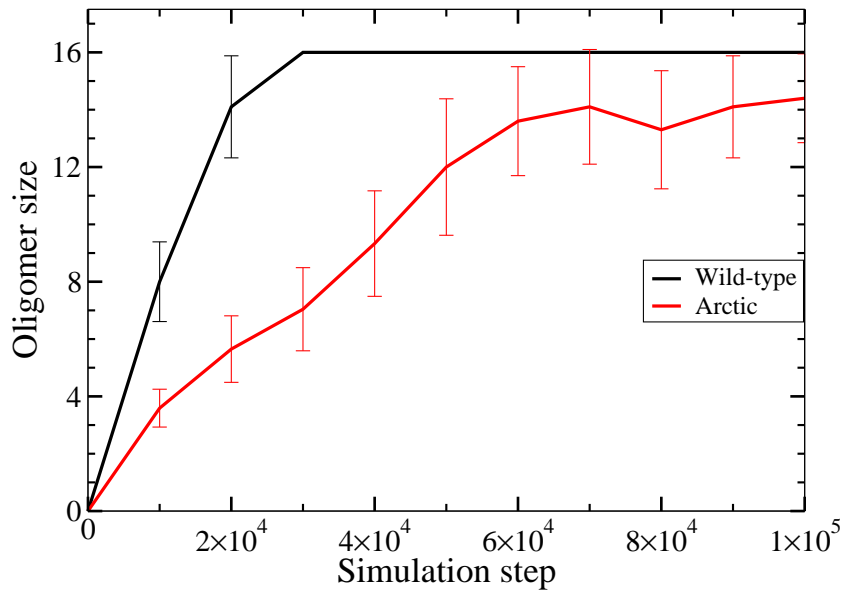


(b) No EI

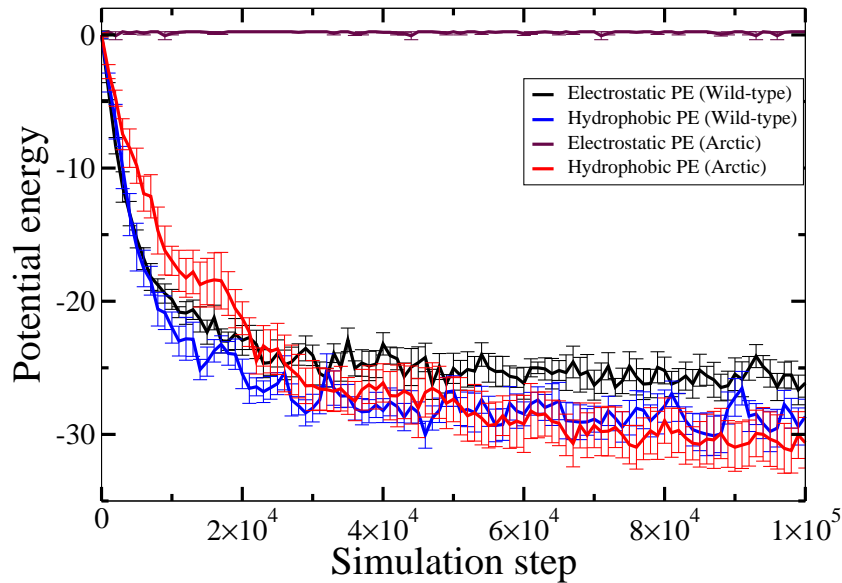


(c) Arctic

Figure 7:



(a)



(b)

Figure 8:

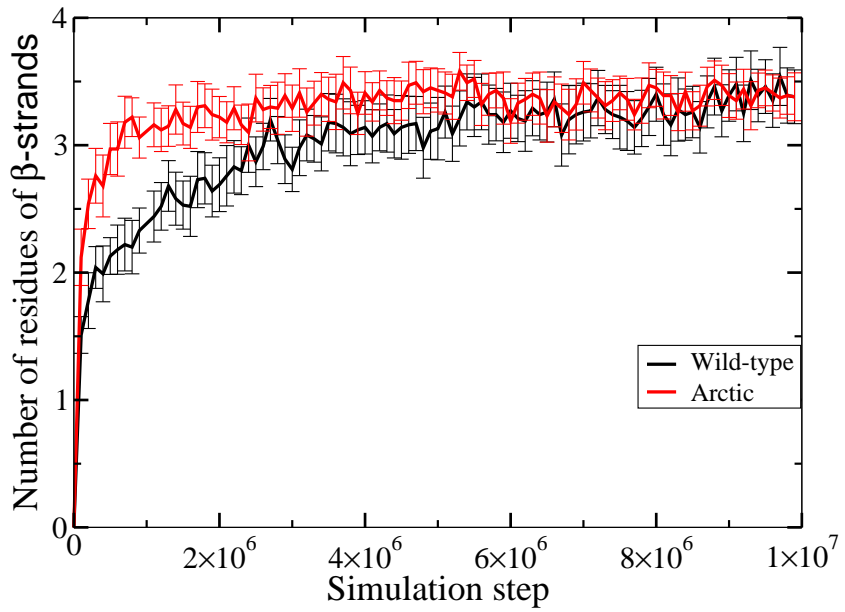


Figure 9: